

Dispersion Anomalies in Bilayer Cuprates and the Odd Symmetry of the Magnetic Resonance

M. Eschrig¹ and M. R. Norman²

¹*Institut für Theoretische Festkörperphysik, Universität Karlsruhe, 76128 Karlsruhe, Germany*

²*Materials Science Division, Argonne National Laboratory, Argonne, Illinois 60439*

(Dated: June 27, 2002)

We present a theoretical model which accounts for recent angle resolved photoemission data in bilayer cuprate superconductors. Lineshapes and dispersions of the various bonding and antibonding features in the spectra are quantitatively reproduced. The observed dispersion anomalies are consistent with the interaction of electrons with a bosonic mode which is odd with respect to the layer indices, a unique property of the magnetic resonance observed by inelastic neutron scattering.

PACS numbers: 74.25.Jb, 74.72.Hs, 79.60.Bm

Recent angle resolved photoemission (ARPES) experiments on bilayer cuprate superconductors were able for the first time to resolve a bilayer splitting between bonding and antibonding bands [1, 2, 3, 4]. The dispersion near the $(\pi, 0)$ point of the Brillouin zone shows an unusual asymmetry between bonding and antibonding self energy effects. In particular, Feng *et al.* [1] found that the energy distribution curves (EDCs, taken at constant momentum) in overdoped $\text{Bi}_2\text{Sr}_2\text{CaCu}_2\text{O}_{8+\delta}$ ($T_c = 65\text{K}$) consist of three features: an antibonding band (AB) peak near 20 meV, a bonding band (BB) peak near 40 meV, and a bonding hump near 105 meV. Recently, Gromko *et al.* [2] reported strong self energy effects in the dispersions derived from momentum distribution curves (MDCs, taken at constant energy) in similar samples ($T_c = 58\text{K}$). Near momentum $(k_x, k_y) = (1, 0.13)\pi/a$, an S -shaped dispersion anomaly, discussed previously in Ref. [5], was shown to be present only in the bonding band MDC, at binding energies between 40 meV and 60 meV. In both experiments, a low energy double peak structure in the EDC was only resolvable in the same momentum region.

In this letter, we demonstrate that all of these features can be explained by a model which assumes that low energy scattering of electrons between the bonding and antibonding bands is strong compared to scattering within each of those bands. As scattering events which connect different bilayer bands are odd with respect to permutation of the layers within a bilayer, this implies that the corresponding bosonic excitations which mediate such scattering must be dominant in the odd channel. The magnetic resonance observed in inelastic neutron scattering has exactly this property [6, 7], and moreover has the correct energy to reproduce the observed dispersion anomalies. Thus, the recent ARPES experiments on bilayer cuprates provide independent support for a strong coupling between this resonance and electronic excitations.

If the electrons are phase coherent between the two planes, then the spectra will exhibit separate bonding (b) and antibonding (a) features with (normal state) disper-

sions given by $\xi_{\vec{k}}^{(b)}$ and $\xi_{\vec{k}}^{(a)}$. In the cuprates, the resulting energy splitting is anisotropic [1, 8]

$$\xi_{\vec{k}}^{(a)} - \xi_{\vec{k}}^{(b)} = \frac{1}{4}t_{\perp}(\cos k_x - \cos k_y)^2. \quad (1)$$

In the superconducting state, the dispersions are modified by the presence of the d -wave order parameter given by $\Delta_{\vec{k}} = \Delta_0(\cos k_x - \cos k_y)$. In agreement with experiment [1, 3], we assume Δ_0 to be the same for the bonding and antibonding bands. Then, the dispersion in the superconducting state takes the form $(E_{\vec{k}}^{(a,b)})^2 = (\xi_{\vec{k}}^{(a,b)})^2 + (\Delta_{\vec{k}})^2$.

This “non-interacting” picture, though, is insufficient to describe the three observed dispersion features. We are able to account for them in a model where electrons are coupled to a resonant spin mode situated below a gapped spin fluctuation continuum. Such a spectrum is observed in inelastic neutron scattering experiments [6]. In bilayer materials, the spin susceptibility is a matrix in the layer indices, having elements diagonal (χ_{aa} , χ_{bb}) and off-diagonal (χ_{ba} , χ_{ab}) in the bonding-antibonding representation. The components of the spin susceptibility transforming as even and odd with respect to the layer indices are given by $\chi_e = \chi_{aa} + \chi_{bb}$ and $\chi_o = \chi_{ab} + \chi_{ba}$. For identical planes, $\chi_{aa} = \chi_{bb}$ and $\chi_{ab} = \chi_{ba}$. The measured susceptibility is then given by

$$\chi = \chi_e \cos^2 \frac{q_z d}{2} + \chi_o \sin^2 \frac{q_z d}{2} \quad (2)$$

where d is the separation of the layers within a bilayer. The resonance part, χ_{res} , was found to exist only in the odd channel, whereas the continuum part, χ_c , enters in both [6]. Thus, $\chi_o = \chi_{res} + \chi_c$ and $\chi_e = \chi_c$. This means the resonance mode can only scatter electrons between the bonding and antibonding bands. In contrast, the spin fluctuation continuum scatters both within and between these bands. As we demonstrate below, the odd symmetry of the resonance is crucial in reproducing the ARPES spectra.

We employ for the single layer self energy the functional form of Ref. [9]. It is proportional to the convolu-

tion of the Gor'kov-Green's function \hat{G} with the dynamic spin susceptibility χ . We write this self energy symbolically as $\hat{\Sigma} = g^2 \chi * \hat{G}$ (the hat denotes the 2x2 particle hole space, and g is the coupling constant). For a bilayer system, there is a separate self energy for each band, $\hat{\Sigma}^{(a,b)}$. Using the above notation, these self energies are given by

$$\hat{\Sigma}^{(b)} = \frac{g^2}{2} \left\{ \chi_{res} * \hat{G}^{(a)} + \chi_c * \left(\hat{G}^{(b)} + \hat{G}^{(a)} \right) \right\} \quad (3a)$$

$$\hat{\Sigma}^{(a)} = \frac{g^2}{2} \left\{ \chi_{res} * \hat{G}^{(b)} + \chi_c * \left(\hat{G}^{(b)} + \hat{G}^{(a)} \right) \right\}. \quad (3b)$$

Dispersion anomalies arise mainly from coupling to the resonance mode. This means that dispersion anomalies in the bonding band are determined by the antibonding spectral function and vice versa. (The spectral functions for the bonding and antibonding bands are given by the imaginary parts of the diagonal components of the Green's functions.) Because the antibonding band is (in contrast to the bonding band) close to the chemical potential at $(\pi, 0)$ [1], the associated van Hove singularity leads to a larger self energy for the bonding band.

The self energy effects can be described very accurately by using a model spin spectrum which consists of a perfectly sharp resonance mode below a gapped continuum with gap Δ_h . We approximate the intensity of the continuum to be constant. In reality, the intensity of the continuum decays at high energies. However, as we are interested in self energy effects in an energy range $|\epsilon| < 200$ meV, the above approximation is adequate. A high frequency cut-off in the convolution integrals in Eqs. (3a) and (3b) was introduced. The precise cut-off procedure however does not affect the low energy physics. Any variation in the cut-off can be accounted for by a readjustment of the coupling constants and the normal state renormalization factor. We model the resonance mode, $R = 2\text{Im}\chi_{res}$, and the continuum, $C = 2\text{Im}\chi_c$, by

$$R_{\omega, \vec{q}} = 2r(\vec{q}) \{ \delta(\omega - \Omega_{res}) - \delta(-\omega - \Omega_{res}) \}, \quad (4a)$$

$$C_{\omega, \vec{q}} = 2c(\vec{q}) \{ \Theta(\omega - 2\Delta_h) - \Theta(-\omega - 2\Delta_h) \}. \quad (4b)$$

where the Θ function is zero for negative argument and one otherwise. The momentum dependences of the resonance mode and the continuum, given by the functions $r(\vec{q})$ and $c(\vec{q})$, are plotted in Fig. 1. The resonance mode, shown in Fig. 1a, is peaked at \vec{Q} , with a correlation length of $\xi_{res} = 2a$, where a is the lattice constant. The gapped continuum, shown in Fig. 1b, is much broader. This is motivated by the experimental data [6], which show that the continuum is enhanced around \vec{Q} with a correlation length of only 0.5 lattice constants. Also, the momentum dependence of the continuum excitations exhibit experimentally a flat behavior around \vec{Q} , as in Fig. 1b. To simplify the model, we use the same functional form for the gapped continuum in the even and odd scattering channels. This is consistent with the superconducting state data, where the gap in the odd channel (about twice the

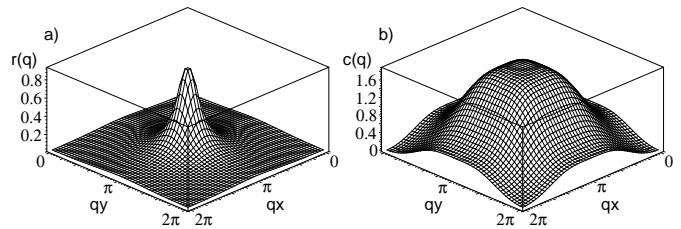


FIG. 1: Momentum dependence of a) the resonance mode and b) the gapped spin fluctuation continuum. The resonance mode is peaked at $\vec{Q} = (\pi, \pi)$ with a correlation length equal to twice the lattice constant, $\xi_{res} = 2a$. The continuum spectrum, in contrast, is rather broad around \vec{Q} .

maximal superconducting gap), is close to the optical gap in the even channel.

We have chosen parameters appropriate for the overdoped sample ($T_c = 65$ K) studied in experiment [1]. The normal state dispersion is obtained from a 6 parameter tight-binding fit to experimental data [11], with the bilayer splitting given by Eq. 1. In order to determine the total of 7 parameters for this fit, we used three Fermi wavevectors, $\vec{k}_N = (0.37, 0.37)\pi/a$, $\vec{k}_A^{(b)} = (1, 0.217)\pi/a$, and $\vec{k}_A^{(a)} = (1, 0.135)\pi/a$, the Fermi velocity at \vec{k}_N , $\vec{v}_N = 2.316$ eV \AA , and the normal state band energies at $(\pi, 0)$, $\xi_M^{(b)} = -105$ meV and $\xi_M^{(a)} = -18$ meV (the corresponding bilayer splitting is $\xi_M^{(a)} - \xi_M^{(b)} = t_\perp = 87$ meV). Finally, to obtain the correct overall shape of the dispersion, we fixed the band energy at (π, π) , using a reasonable value $\xi_Y = 0.8$ eV. The high energy ($|\epsilon| \gtrsim 200$ meV) dispersions are not affected strongly when going from the normal to the superconducting state. However, even in the normal state, the bare dispersion is renormalized by the normal state spin fluctuation continuum. To account for this renormalization, we multiply the above dispersion by a factor of 1.4 in order to obtain the bare dispersion. For the remaining parameters of the model, we use $\Delta_0 = 16$ meV [1], $\Omega_{res} = 27$ meV, $\Delta_h = 0.9\Delta_0$, $g^2r(\vec{Q}) = 0.15\text{eV}^2$, and $g^2c(\vec{Q}) = 0.72\text{eV}$. The value for the resonance energy was obtained from the relation $\Omega_{res} = 4.9k_B T_c$ found experimentally to hold for overdoped $\text{Bi}_2\text{Sr}_2\text{CaCu}_2\text{O}_{8+\delta}$ [6, 7, 12]. The resonance weight $r(\vec{Q})$ has not been measured for overdoped materials. For optimally doped $\text{Bi}_2\text{Sr}_2\text{CaCu}_2\text{O}_{8+\delta}$, it is $0.95\mu_B^2$ per plane [7], and we estimated for this case $g = 0.65$ eV [9]. Assuming for the overdoped sample the same coupling constant, the above value for $g^2r(\vec{Q})$ would imply a resonance weight of $0.36\mu_B^2$ per plane. Similarly, with this coupling constant and our value for $g^2c(\vec{Q})$, we obtain a (2D)-momentum averaged continuum contribution of $1.7\mu_B^2/\text{eV}$ per plane (gotten by summing the even and odd channels for energies $\omega \lesssim 0.2\text{eV}$). Our calculations are for a temperature $T = 10$ K. Note we use unrenormalized Green's functions in Eqs. 3a and 3b. This

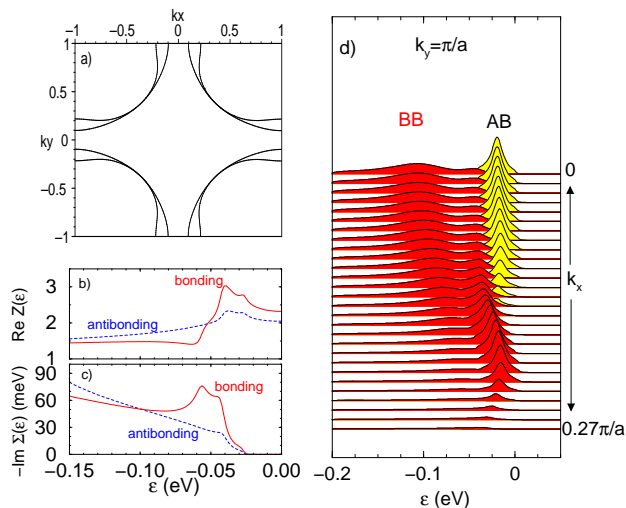


FIG. 2: a) Tight binding Fermi surfaces for antibonding and bonding bands in overdoped $\text{Bi}_2\text{Sr}_2\text{CaCu}_2\text{O}_{8+\delta}$ ($T_c = 65\text{K}$). b) Renormalization function and c) imaginary part of the self energy at the $(\pi, 0)$ point of the zone for the bonding band (BB) and antibonding band (AB). d) Spectral functions for $k_y = \pi/a$, and k_x varying from 0 to $0.27\pi/a$. For comparison with experiment, the spectra are convolved with a Lorentzian energy resolution function (FWHM 12 meV).

approximation is sufficient to explain a large variety of data, and can be justified by considerations discussed in Ref. [10].

The bonding and antibonding normal state Fermi surfaces are shown in Fig. 2a. The bilayer splitting is maximal near the $(\pi, 0)$ points of the zone. Thus, we will concentrate on this region in the following. In Fig. 2b we show the renormalization function for bonding and antibonding bands at the $(\pi, 0)$ point. The renormalization is stronger for the bonding band than the antibonding band. This is a result of the proximity of the antibonding saddle point singularity to the chemical potential. As is seen in this figure as well, both bands are renormalized up to high energies. The high energy renormalization approaches that of the normal state dispersion (1.4).

The imaginary part of the self energy is shown in Fig. 2c for the bonding and antibonding bands. As emission processes are forbidden for $|\epsilon| < \Omega_{res}$, the imaginary part of the self energy is zero in this range. Due to scattering events to the antibonding band, electrons in the bonding band have a large imaginary part of the self energy in the range between 40 and 60 meV. These events are dominated by emission of the resonance, and are enhanced due to the van Hove singularity in the antibonding band close to the chemical potential. In contrast, the imaginary part of the antibonding self energy is not enhanced because the bonding band is far away from the chemical potential at $(\pi, 0)$. Consequently, it shows linear behavior over a wide energy range, with a gap at low

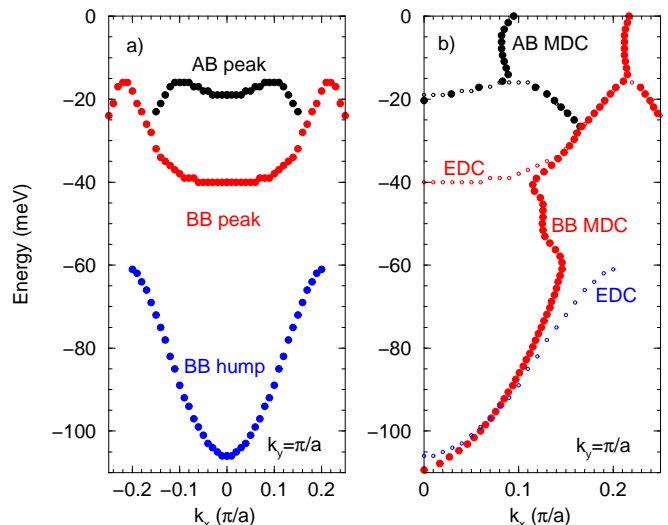


FIG. 3: Dispersion of EDC peak positions (left) and MDC peak positions (right) near the $(\pi, 0)$ point of the Brillouin zone. The EDC dispersion consists of three branches, one antibonding peak, one bonding peak and one bonding hump. The MDC bonding dispersion shows a characteristic *S* shape behavior. The small symbols in the right picture show again the EDC peak positions for convenience.

energies ($|\epsilon| < \Omega_{res}$).

Fig. 2d presents the intensities for the bonding and antibonding spectra. The antibonding spectra consist of a low energy AB peak, and the bonding spectra have a low energy BB peak and a higher energy BB hump feature. In agreement with experiment ([1] and [2]), the width of the EDC spectrum is large for the BB hump, but not so for the BB and AB peaks. We also mention that the BB peak is well defined in the whole region between the BB Fermi crossings on either side of $(\pi, 0)$, but the finite energy resolution does not allow to resolve it near $(\pi, 0)$ as seen in Fig. 2d.

In Fig. 3 we show our results for dispersion of the EDC and MDC peak positions. In the EDC dispersions, Fig. 3a, we reproduce the experimentally observed three branches [1], one antibonding peak and two bonding branches, denoted ‘BB peak’ and ‘BB hump’. The BB peak has a very flat dispersion near $k_x = 0$ in agreement with experiment [1]. Its position at 40 meV is approximately given by $\Omega_{res} + \Delta_A$, where Δ_A is the gap at the antibonding Fermi crossing. Thus, the energy separation between the AB peak at the AB Fermi crossing and the BB peak at $(\pi, 0)$ is a measure of the resonance mode energy Ω_{res} in overdoped compounds. The BB hump position at high binding energies (105 meV) is determined by the normal state dispersion of the bonding band. Because the spin fluctuation continuum changes only at low energies when going from the normal to the superconducting state, the position of the BB hump maximum is not very different from the normal state BB dispersion. This is in

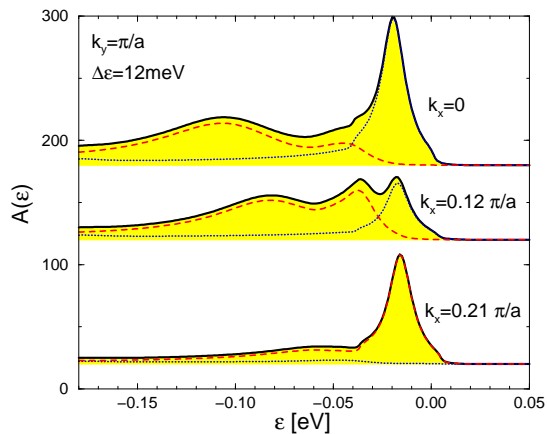


FIG. 4: Spectral functions for $k_y = \pi/a$ at $k_x = 0$, $k_x = 0.12\pi/a$ and $k_x = 0.21\pi/a$. The full lines are the sum of antibonding (dotted) and bonding (dashed) spectral functions. For comparison with experiment, a Lorentzian energy resolution function of 12 meV width was assumed. The double peak structure is clearly resolved for $k_x = 0.12\pi/a$, as in experiment [1, 2].

agreement with experiment [1]. The intensity of the AB peak decreases quickly when it approaches the BB peak, but is strong at $(\pi, 0)$ because of the proximity of the AB band to the chemical potential in this region.

In Fig. 3b, we present the MDC dispersions (for comparison we also reproduce the EDC dispersions as small symbols). The MDC dispersion consists of two branches, an AB MDC branch and a BB MDC branch. The self-energy effects are most clearly observable in the BB MDC branch. In the binding energy range between 40meV and 60meV, there is an *S*-shaped ‘break’ region, connecting the BB hump EDC branch with the BB peak EDC branch. This *S*-shaped behavior reproduces the finding of recent experiments [2].

The dispersion anomalies observed in the *bonding* band are a mirror of the large number of states close to the chemical potential near $(\pi, 0)$ for the *antibonding* band. Scattering events involving a mode with energy Ω_{res} couple the bonding band electrons in the energy region between 40 and 60 meV strongly to those antibonding band electrons. The corresponding processes are in the odd scattering channel. The energy range of anomalous dispersion is shifted by the resonance mode energy with respect to the antibonding binding energies.

Finally, in Fig. 4 we compare spectra for three positions in the Brillouin zone, corresponding to the spectra presented in Refs. [1, 2]. For each spectrum, the bonding (dashed) and antibonding (dotted) contributions are

indicated. The spectra are convolved with a Lorentzian energy resolution function to allow for direct comparison with experiment. We reproduce all experimental findings. First, at $(\pi, 0)$, only the BB hump and the AB peak are resolved. This is due to resolution effects mentioned above. Second, near the AB Fermi crossing, the spectra show a characteristic double peak structure, with a relatively sharp AB peak and a BB peak separated from a broad BB hump. Third, at the BB Fermi crossing, only the BB peak is observed. The BB hump is so small in intensity that it only leads to a kink-like feature in the spectrum.

We have presented a theory to account for the experimentally observed self energy effects in the bilayer split bands in double layer high temperature superconductors. We reproduced quantitatively the EDC dispersions, the MDC dispersions, and the spectral lineshapes. We found that the ARPES data are consistent with the interaction of the electrons with a sharp bosonic mode which is odd in the layer indices, a property unique to the magnetic resonance observed by inelastic neutron scattering.

This work was supported by the U. S. Dept. of Energy, Office of Science, under Contract No. W-31-109-ENG-38.

-
- [1] D.L. Feng *et al.*, Phys. Rev. Lett. **86**, 5550 (2001) and Phys. Rev. B **65**, 220501 (2002).
 - [2] Y.-D. Chuang *et al.*, Phys. Rev. Lett. **87**, 117002 (2001) and cond-mat/0107002; A.D. Gromko *et al.*, cond-mat/0202329 and cond-mat/0205385.
 - [3] A.A. Kordyuk *et al.*, Phys. Rev. B **66**, 014502 (2002) and cond-mat/0110379; S.V. Borisensko *et al.*, cond-mat/0204557.
 - [4] A. Kaminski *et al.*, unpublished.
 - [5] M.R. Norman *et al.*, Phys. Rev. B **64**, 184508 (2001).
 - [6] J. Rossat-Mignot *et al.*, Physica C **185-189**, 86 (1991); H.A. Mook *et al.*, Phys. Rev. Lett. **70**, 3490 (1993); H.F. Fong *et al.*, *ibid.* **75**, 316 (1995) and Phys. Rev. B **61**, 14773 (2000); P. Dai *et al.*, *ibid.* **63**, 054525 (2001).
 - [7] H.F. Fong *et al.*, Nature (London) **398**, 588 (1999); H. He *et al.*, Phys. Rev. Lett. **86**, 1610 (2001).
 - [8] S. Chakravarty *et al.*, Science **261**, 337 (1993); O. K. Andersen *et al.*, J. Phys. Chem. Solids **56**, 1573 (1995).
 - [9] M. Eschrig and M.R. Norman, Phys. Rev. Lett. **85**, 3261 (2000) and cond-mat/0202083.
 - [10] Y.M. Vilks and A.-M.S. Tremblay, J. Phys. France **7**, 1309 (1997).
 - [11] M.R. Norman *et al.*, Phys. Rev. B **52**, 615 (1995); parameters used here are (eV): $t_0 = 0.1129$, $t_1 = -0.6581$, $t_2 = 0.0707$, $t_3 = -0.1465$, $t_4 = -0.0620$, $t_5 = 0.0428$.
 - [12] J.F. Zasadzinski *et al.*, Phys. Rev. Lett. **87**, 067005 (2001).